



KTH ROYAL INSTITUTE OF TECHNOLOGY

---

# Investigating Urea Vaporization in a Controlled Environment Using Infrared Thermography

KE202X Degree Project in Chemical Engineering, Second Cycle, 30 credits

---

*Author:*  
Henrik GRIMLER

*Supervisor:*  
Henrik BIRGERSSON, Ph D.

*Examiner:*  
Prof. Lars PETTERSSON

July 2, 2015



**SCANIA**

## Abstract

As the emission legislation becomes more stringent, higher demands are put on the aftertreatment system in trucks. For dealing with nitrous oxides, AdBlue<sup>®</sup> (urea–water solution) is injected into the exhausts which evaporates and reduces nitrous oxides to nitrogen. At low exhaust temperatures, it is more difficult to evaporate the injected AdBlue<sup>®</sup> as the exhausts contain less energy. The injected solution may instead form a wall film. In this wall film, side reactions can occur which leads to the formation of deposits.

This thesis aims at understanding how and when wall films and deposits are formed. To achieve this, a test rig that allowed visual and infrared observations of the process and variation of governing properties was designed and built.

The results show that thicker plates can sustain higher dosages than thinner plates since the temperature drop and film area are smaller for the thicker plate. It was also observed that at plate temperatures  $\gtrsim 340\text{ }^{\circ}\text{C}$ , the water in the impacting spray evaporated, leaving a urea dust in the gas phase.

It is also clear that deposits form faster at higher gas temperatures ( $\gtrsim 350\text{ }^{\circ}\text{C}$ ) compared to at lower temperatures ( $200\text{--}250\text{ }^{\circ}\text{C}$ ). The deposits form at the edge of the wall film in a region with a temperature higher than in the middle of the wall film. At lower temperatures, a wall film that spreads out over a very large area is formed and after a longer time period, deposits form at obstacles and at the wall film edge. Experiments for 2 h at lower temperatures left approximately the same amount of deposits as experiments for 30 min at higher temperatures.

## Sammandrag

När lagkraven blir strängare sätts högre krav på efterbehandlingssystemet i lastbilar. För att få bort nitrösa gaser injiceras AdBlue<sup>®</sup> (urea-vattenlösning) in i avgaserna vilken förångas och reducerar de nitrösa gaserna till ofarligt kväve. Vid låga avgastemperaturer är det svårare att förånga den injicerade AdBlue<sup>®</sup>-lösningen då avgaserna innehåller mindre energi. Den injicerade lösningen kan istället bilda en väggfilm. I denna väggfilm kan sidoreaktioner ske vilket leder till bildning av utfällningar.

Detta examensarbete syftar till att öka förståelsen för hur och när väggfilmer och utfällningar bildas. För att uppnå detta designades och byggdes en testrigg i vilken visuella och infraröda observationer kan göras och influerande parametrar varieras.

Resultaten visar att tjockare plåtar kan utstå högre doseringar jämfört med tunnare plåtar, eftersom lägre temperaturminskning och film area uppmätts för den tjockare plåten. Det sågs också att vid plåttemperaturer  $\gtrsim 340\text{ }^{\circ}\text{C}$  så förångades vattnet i AdBlue<sup>®</sup>-lösningen först och efterlämnade ett ureadamm i gasfasen.

Det konstaterades också att utfällningar bildas snabbare vid högre gastemperaturer ( $\gtrsim 350\text{ }^{\circ}\text{C}$ ) jämfört med vid lägre temperaturer ( $200\text{--}250\text{ }^{\circ}\text{C}$ ). Utfällningarna bildas vid kanten av väggfilmen i en region som har en temperatur som är högre än den i mitten av väggfilmen. Vid lägre temperaturer bildas en väggfilm som sprider ut sig över en stor area och med tiden bildas utfällningar vid hinder och vid filmkanten. Experiment under 2 h vid låg gastemperatur gav jämförbara mängder utfällningar som experiment under 30 min vid högre temperatur.

### **Acknowledgments**

I would like to dedicate this master thesis to my family and to my girlfriend, Caroline. Thanks for always being supportive in all of my endeavors.

Thanks everyone on NMTU for answering questions and including me in the group. Lastly, special thanks to my supervisor Henrik for all the support and to my examiner, Lars, for interesting insights and stories during the past years.

Stockholm, June 2015

A handwritten signature in black ink, appearing to read 'Henrik Grimler', written in a cursive style.

*Henrik Grimler*

# Contents

<b>Abstract</b>	<b>ii</b>
<b>Sammandrag</b>	<b>iii</b>
<b>Acknowledgments</b>	<b>iv</b>
<b>1 Introduction</b>	<b>1</b>
1.1 Formation of Nitrogen Oxides . . . . .	1
1.2 Urea Selective Catalytic Reduction . . . . .	3
1.2.1 Urea Decomposition . . . . .	3
1.2.2 Urea Evaporation . . . . .	3
1.2.3 Model for Wall Interaction . . . . .	5
1.2.4 Nitrogen Oxide Reduction in the Selective Catalytic Reduction Catalyst .	7
1.3 Other Techniques for Reduction of Nitrogen Oxides . . . . .	7
1.3.1 Exhaust Gas Recirculation . . . . .	7
1.3.2 Hydrocarbon Selective Catalytic Reduction . . . . .	8
1.3.3 Lean NO <sub>x</sub> Trap . . . . .	8
1.4 Heat Transfer Theory . . . . .	9
1.5 Previous Research and Experiments . . . . .	10
1.5.1 Previous Test Rigs . . . . .	10
1.6 Motivation . . . . .	11
1.7 Aims and Goals . . . . .	11
<b>2 Experiments</b>	<b>12</b>
2.1 Experimental Design . . . . .	12
2.1.1 Desired Properties of the Test Rig . . . . .	12
2.1.2 Test Rig Design . . . . .	12
2.2 Experimental Setup . . . . .	13
2.2.1 The Injector . . . . .	15
2.2.2 The Infrared Camera . . . . .	15
<b>3 Results and Discussion</b>	<b>17</b>
3.1 Influence of Plate Properties on Evaporation Performance . . . . .	17
3.1.1 Effect of Tilting Plate . . . . .	17
3.1.2 Effect of Changing Thickness of Plate . . . . .	18
3.2 Influence of Gas Flow on Evaporation Performance . . . . .	18
3.3 Influence of Gas Temperature on Evaporation Performance . . . . .	19

3.4	Instantaneous Evaporation . . . . .	20
3.5	Temperature Recovery of the Plates . . . . .	22
3.6	Deposit Formation at Different Temperatures . . . . .	22
<b>4</b>	<b>Conclusions</b>	<b>24</b>
4.1	Recommendations for Future Work . . . . .	24
	<b>Acronyms</b>	<b>26</b>
	<b>List of Symbols</b>	<b>27</b>
	<b>Subscripts</b>	<b>28</b>
	<b>References</b>	<b>29</b>

# List of Figures

1.1	NO <sub>x</sub> -Legislated Limit Timeline . . . . .	2
1.2	Droplet-Wall Interaction . . . . .	4
1.3	Proposed Schemes for Droplet-Wall Interaction in Literature . . . . .	6
1.4	Aftertreatment System . . . . .	7
1.5	Temperature Profile of Exhaust Gas Wall . . . . .	9
2.1	Blueprint of Test Rig . . . . .	13
2.2	Photo of Test Rig . . . . .	13
2.3	IR-camera Photo . . . . .	14
2.4	Method for Area Calculation . . . . .	14
2.5	Thick Tilted Plate Dimensions . . . . .	15
2.6	Geometry of the Injector and Plate . . . . .	15
2.7	Experiment Plan . . . . .	16
3.1	$\Delta T$ and Area for Thick and Tilted Thick Plates . . . . .	17
3.2	$\Delta T$ and Area for Thin and Thick Plates . . . . .	18
3.3	$\Delta T$ and Area for Different Gas Flow Rates . . . . .	19
3.4	$\Delta T$ and Area for Different Gas Temperatures . . . . .	19
3.5	Minimum Temperature During Dosing for Thick Plate . . . . .	20
3.6	Minimum Temperature During Dosing for Thin Plate . . . . .	21
3.7	Temperature Recovery of Plates . . . . .	22

# Chapter 1

## Introduction

As the emission legislation all over the world becomes more stringent, truck manufacturers are forced to implement and develop aftertreatment systems that can deal with Nitrogen Oxides ( $\text{NO}_x$ ). Several techniques, more or less successful, exist which are described in *Section 1.3*. *Figure 1.1* shows how the European legislated limits for  $\text{NO}_x$ -emissions have changed since they were first introduced.

The emission limits in *Figure 1.1* are mean values of  $\text{NO}_x$  released during standardized test cycles. For Euro VI, the World Harmonized Stationary Cycle (WHSC) and World Harmonized Transient Cycle (WHTC) are used. The stationary cycle examines performance with constant loads by keeping the load constant at different loads of interest for different amount of times. In the transient cycle, the load is varied to simulate three types of driving conditions: urban, rural and highway driving.

Lower  $\text{NO}_x$ -limits demand more sophisticated systems for  $\text{NO}_x$ -treatment and more sophisticated systems create new problems for manufacturers to address. Traditionally, techniques like Exhaust Gas Recirculation (EGR) has been used successfully to keep  $\text{NO}_x$  emissions below the legislated limits but after EU IV was introduced there was a need for additional aftertreatment to reduce  $\text{NO}_x$ .

### 1.1 Formation of Nitrogen Oxides

$\text{NO}_x$  can be produced by four mechanisms. The total  $\text{NO}_x$  concentration can be ascribed to:

- Thermal  $\text{NO}_x$
- $\text{NO}_x$  via  $\text{N}_2\text{O}$
- Prompt  $\text{NO}_x$
- Fuel  $\text{NO}_x$

Formation of *Thermal  $\text{NO}_x$*  requires a high temperature. It becomes important only above 1400 °C and thus happens in the engine at the warmest zone of the gas mixture. This is at the flame boundary, where combustion occurs. The mechanism is called the extended Zeldovich mechanism from the original discoverer and is shown in *Reaction R 1.1 to R 1.3* [2].



*$\text{NO}_x$  via  $\text{N}_2\text{O}$*  is created through the mechanism in *Reactions R 1.4 to R 1.6* [2].



Where M is any molecule that can absorb vibrational energy from the product  $\text{N}_2\text{O}$ . Without M,  $\text{N}_2\text{O}$  would decompose into its reactants. The formed  $\text{N}_2\text{O}$  from *Reaction R 1.4* generally decomposes through

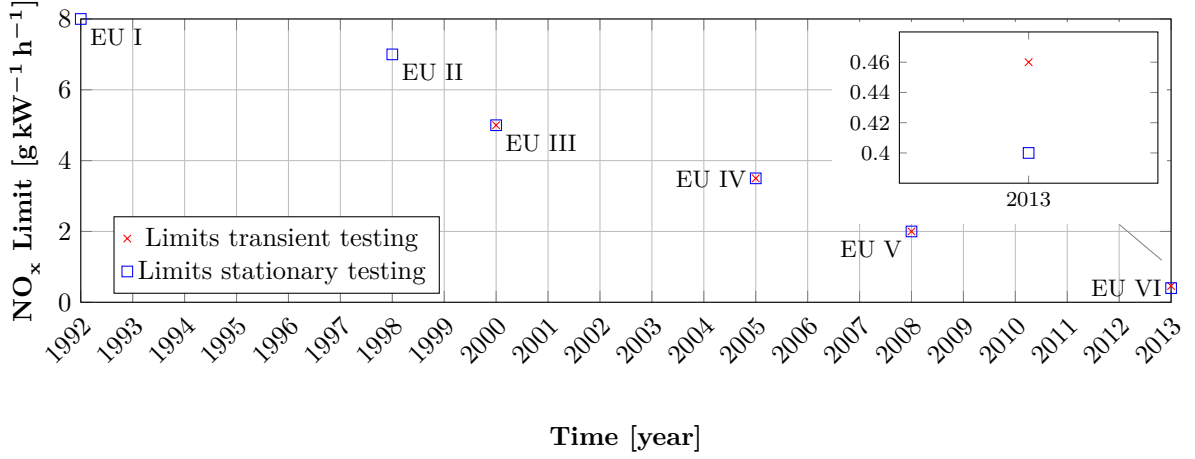
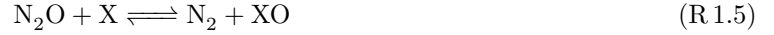


Figure 1.1: Timeline of how the legislated emission limits have changed since they were introduced in Europe. All limits are identical except the one in 2013 [1].

*Reaction R 1.5* by reacting with X (a radical).



Under lean conditions,  $\text{N}_2\text{O}$  can also react with an oxygen radical through *Reaction R 1.6* and generate  $\text{NO}_x$ .



*Prompt  $\text{NO}_x$*  comes from reactions with hydrocarbon radicals



Followed by several reactions



Both of the nitrogen atoms in *Reaction R 1.7* can thus end up as NO through *Reactions R 1.8* to *R 1.11*. Since the reaction mechanism is started from hydrocarbon radicals, the concentration of hydrocarbons is crucial for the rate of prompt  $\text{NO}_x$  formation. With less hydrocarbons, less prompt  $\text{NO}_x$  are therefore formed. Diesel engines run under lean conditions and therefore concentrations of hydrocarbons are low and this mechanism is less important [3].

*Fuel  $\text{NO}_x$*  is formed if the fuel contains nitrogen bound to the fuel. This nitrogen will be combusted into NO in the engine by one of two possible routes, depending on how nitrogen is bound. It can either be situated in an aromatic ring or in an amine group. If the nitrogen is present within an aromatic ring, it will first react to HCN and then follow the same mechanism described by *Reaction R 1.8* to *R 1.11*. If it is present in an amine group, it will form ammonia which can then react through *Reaction R 1.12* to *R 1.16* [3].



where X is any radical.

In diesel engines, the most important mechanisms contributing to the total  $\text{NO}_x$  emissions are the thermal  $\text{NO}_x$  mechanism and  $\text{NO}_x$ -production via  $\text{N}_2\text{O}$  [4].

## 1.2 Urea Selective Catalytic Reduction

Urea for urea-Selective Catalytic Reduction (SCR) is kept on-board as a 32.5 wt-% water solution. It is sold as AdBlue® in Europe. AdBlue® is a solution that is easy and safe to handle. It is, however, not urea that is the active reducing agent in the deNO<sub>x</sub>-reactions. Urea is decomposed into ammonia and it is ammonia that reduces NO<sub>x</sub> in the SCR-catalyst.

### 1.2.1 Urea Decomposition

Ammonia is produced from urea through several steps. First, the AdBlue® solution is injected into the exhaust gas stream as small droplets. Heat is transported to the droplets, which makes water evaporate since water has a higher vapor pressure than urea. This increases the urea concentration in the droplets and the higher temperature and concentration increases the reaction rates for different reactions. The desired reaction of urea is thermolysis to cyanic acid and ammonia followed by hydrolysis of cyanic acid to carbon dioxide and ammonia as depicted in *Reaction R 1.17*.

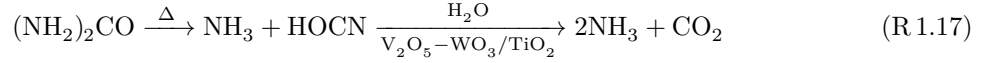
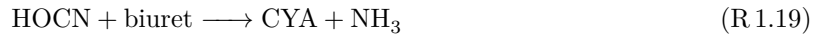


Table 1.1: Properties of urea and AdBlue®

Property	Value	Source
T(melting)	132–137 °C	[5, 6]
T(evaporation)	223 °C	[5]
T(decomposition)	158 °C	[5]
Molecular weight	60.06 kg kmol <sup>-1</sup>	[7]
Density (AdBlue®, 20 °C)	1335 kg m <sup>-3</sup>	[7]
Solubility (17 °C)	100 g · (100 g H <sub>2</sub> O) <sup>-1</sup>	[7]

Depending on the conditions, i.e. temperature and heat transfer rate, the thermolysis in *Reaction R 1.17* can either happen from aqueous (NH<sub>4</sub><sup>+</sup> + <sup>-</sup>OCN), solid or molten urea [8, 9]. The hydrolysis takes place in the gas phase or in the SCR catalyst. However, the hydrolysis in gas phase only becomes significant at temperatures above 400 °C since HOCN is stable as a gas [10, 11].

If a wall film is created, side reactions can take place which lead to the formation of deposits. One possible reaction is that of dissolved HOCN reacting with urea forming biuret (NH<sub>2</sub>CONHCONH<sub>2</sub>), as depicted in *Equation (R 1.18)*. If HOCN instead reacts with an already created biuret molecule, Cyanuric Acid (CYA) is formed, as in *Reaction R 1.19*. CYA and biuret can react further to heavier compounds to form insoluble, stable molecules that deposit in the exhaust gas system and increase the pressure drop [9]. It is hence these heavier compounds that are problematic. Both biuret and CYA can decompose if the temperature is raised to 230 °C and 370 °C, respectively [5].



### 1.2.2 Urea Evaporation

Grout et al. [12] showed that a droplet with a diameter of 150 µm needs to travel with the exhaust gases about 3 m to evaporate under low load conditions if all heat is transported to the droplet by convection. This means that virtually all droplets will reach a wall since the pipe where urea is evaporated is much shorter, e.g. only 35 cm in a Scania muffler of the medium type. When the droplet comes in contact with a wall, heat can be transported to it by conduction – which increases the rate of evaporation. If the wall temperature is very high when the droplet hits it, typically above a temperature called the Ledienfrost temperature ( $T_L$ , characteristic for the liquid and surface), the heat flux by radiation and convection from the wall is very high. This high heat flux causes the droplet to start evaporating before reaching the wall.

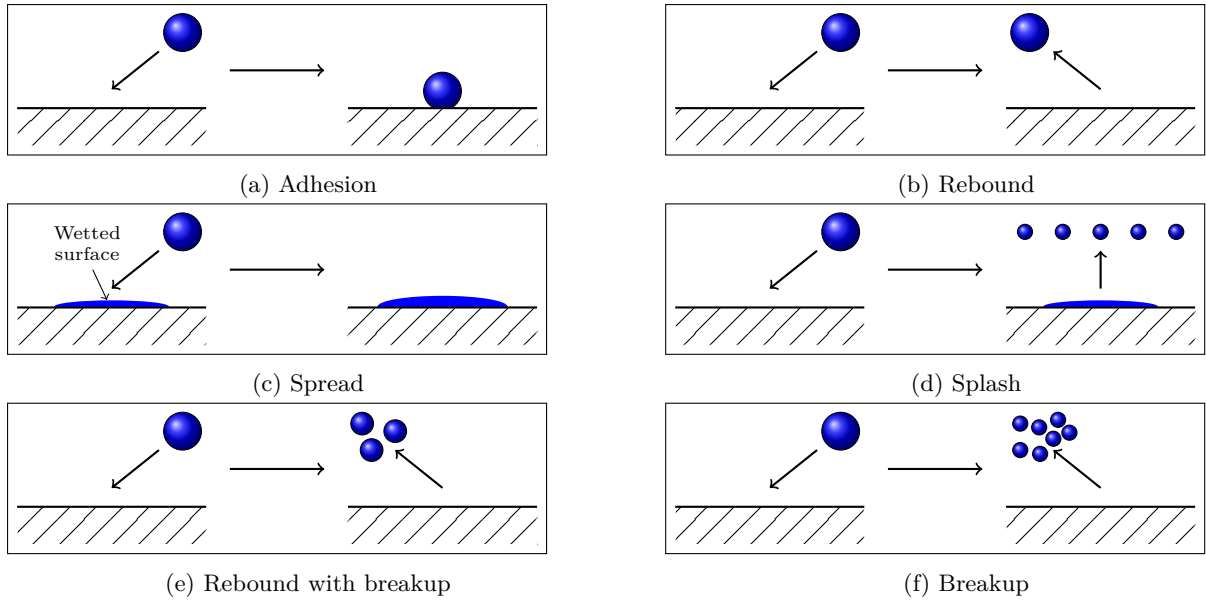


Figure 1.2: Illustration of the different droplet–wall interaction

A vapor cushion is formed beneath the droplet which prevents conduction and lowers the rate of heat transfer.

The heat transferred to the droplet from the wall decreases the inherent energy content in the wall and the temperature of the wall starts to drop. As the temperature falls beneath a threshold value, a liquid film is formed. The rate of heat transfer is enhanced since conduction can take place and this causes the wall temperature to decrease rapidly.

A wall film is not created under all conditions though. A steady state can instead be reached where the heat flux to the wall sustains evaporation of the dosed AdBlue<sup>®</sup>. Many factors influence this process, namely exhaust gas temperature, exhaust gas flow rate, the amount of urea solution injected per unit time and the droplet sizes:

- Higher temperature improves heat transfer to wall and droplets.
- Higher flow rate also improves heat transfer rate to the wall and droplets.
- More injected urea solution means that more energy per unit time is required for evaporation.
- Smaller drops have higher total surface area and smaller inertia, both increases rate of evaporation.

Together, these factors determine if a wall film is created or not.

Depending on the wall temperature, different phenomena can occur when the droplets hit the wall. Chen et al. [13] have presented six possible interaction types:

- i) Adhesion: stick to the wall in an almost spherical form.
- ii) Rebound: bounce off the wall.
- iii) Spread: stick to the already wetted wall as a film.
- iv) Splash: part of the droplet stick to the wall and part of it rebounds as smaller droplets.
- v) Rebound with breakup: low speed droplets bounce back from the hot wall and breaks into two or three smaller droplets.
- vi) Breakup: high-speed droplets break up into many small droplets after colliding with the hot wall.

The different interactions are illustrated in *Figure 1.2*. While the urea droplets cool the wall, heat is transported to it from exhaust gases on the other side of the wall, as illustrated in *Figure 1.5*.

More on heat transfer can be found in *Section 1.4*. Models have been developed to predict which behavior a droplet will exhibit but the field is still evolving quickly with new better models being developed

[14].

### 1.2.3 Model for Wall Interaction

In the literature, models to predict the droplet–wall interaction based on important parameters have been proposed. The wall temperature, the Leidenfrost temperature of the liquid and three dimensionless numbers are commonly used to determine the droplet behavior as it hits a wall. The Leidenfrost temperature is the wall temperature at which an incoming droplet takes the most time to evaporate.

$$We = \frac{\rho u^2 d}{\sigma} \quad (1.1)$$

The Weber number, it is the ratio of inertial forces and surface tension forces.

$$Re = \frac{\rho u d}{\mu_g} \quad (1.2)$$

The Reynolds number, it is the ratio between inertial forces and viscous forces.

$$Oh = \frac{\mu_g}{\sqrt{\rho \sigma d}} = \frac{\sqrt{We}}{Re} \quad (1.3)$$

The Ohnesorge number, representing fluid properties. If  $Oh$  is low, it means that the fluid either has a low viscosity or have a high surface tension.

$$Ca = \frac{u \mu_g}{\sigma} \quad (1.4)$$

The capillary number, it is the ratio of viscous forces to surface tension at a liquid-gas interface. If  $Ca$  is low, it means that the fluid is either highly viscous or have a low surface tension.

In *Equations* (1.1) to (1.4) the different parameters are

Table 1.2: Parameters for droplet–wall interaction model

Parameters	Explanation	Unit
$\rho$	Density of droplet	$\text{kg m}^{-3}$
$u$	Velocity of droplet	$\text{m s}^{-1}$
$d$	Diameter of droplet	m
$\sigma$	Surface tension of droplet–gas interface	$\text{J m}^{-2}$
$\mu_g$	Viscosity of the gas	Pa s

Many authors calculate a number  $K$  on the form  $K = Oh^a \cdot We^b$  and use this as a parameter in the droplet film interaction models. Another important physical quantity is the ratio between the liquid mass hitting the surface and the mass of liquid that bounces back. This ratio is often reported as a function of  $K$ . For example, Mundo et al. [15] gave these correlations for  $K$  and  $\frac{m_a}{m_b}$  (mass of droplets bouncing back divided by mass of droplets hitting the surface):

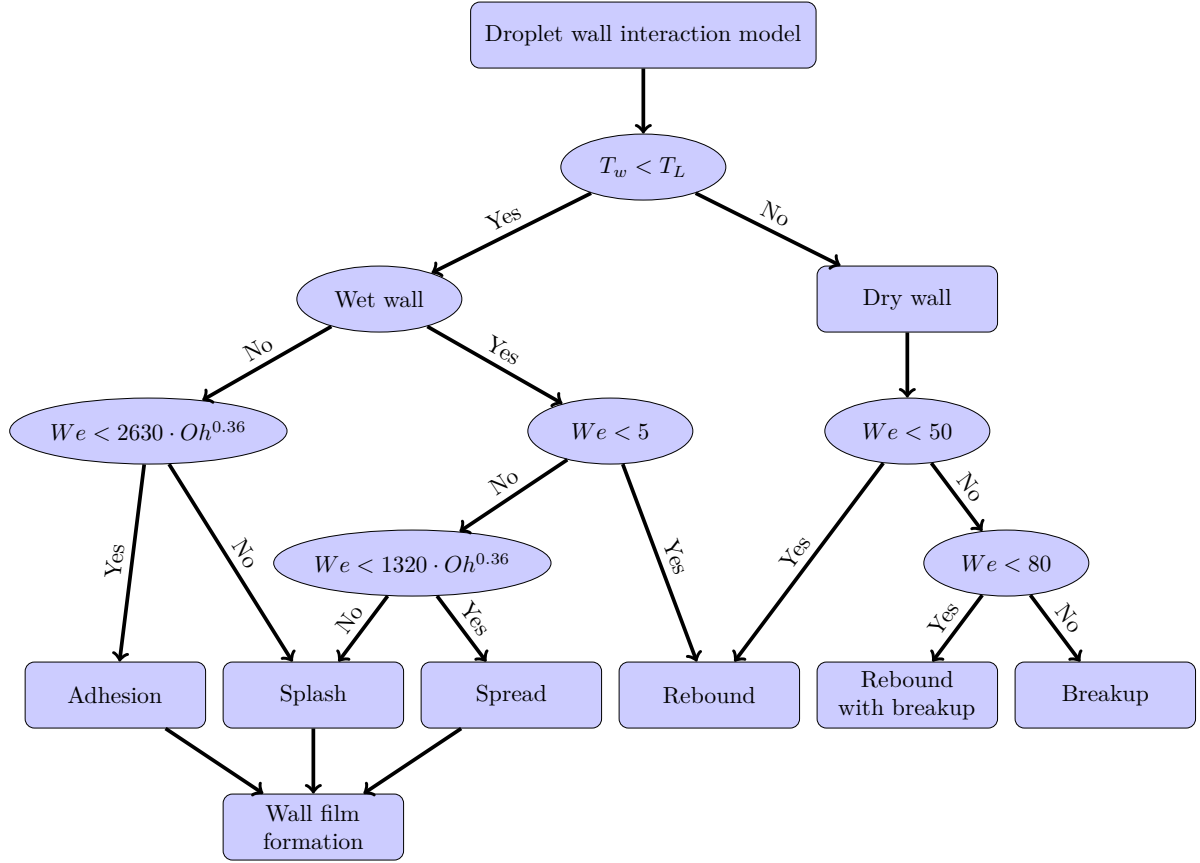
$$K = We^{0.5} Re^{0.25} \quad (1.5)$$

$$\frac{m_a}{m_b} = \begin{cases} 3.9869 \cdot 10^{-21} K^{9.2133} & \text{Smooth wall} \\ 8.0350 \cdot 10^{-11} K^{4.1718} & \text{Rough wall} \end{cases} \quad (1.6)$$

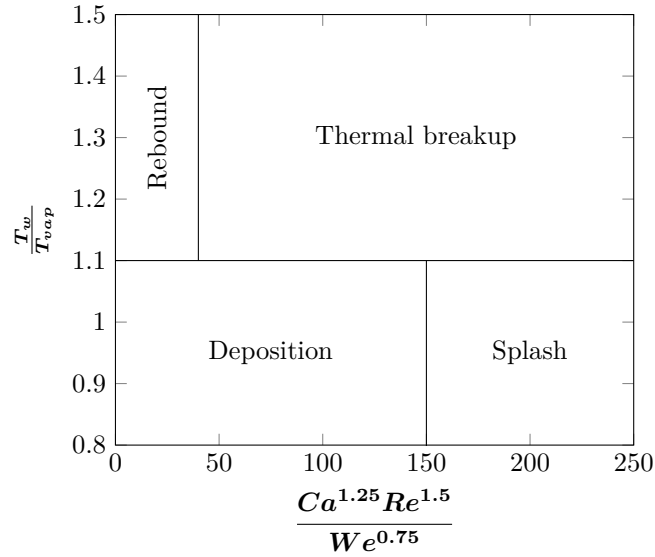
Large differences in predicted behavior under the same conditions exist in the literature though, with very different models [16]. Chen et al. [13] examined the interaction between fuel droplets and the cylinder wall. They presented a scheme for determining the interaction based on experiments by several authors. Since the scheme has been developed for fuel droplets and not urea solution droplets, the scheme should mainly be used to get a qualitative picture of the droplet–wall interaction. The proposed scheme can be seen in *Figure 1.3a*.

A simpler scheme using the wall temperature and the parameter  $K$  has been proposed by Birkhold et al. [17] based on the work by Kuhnke [18]. The scheme is once again based on experiments on fuel sprays and not urea solution sprays but can nevertheless provide a qualitative overview of the droplet–wall interactions. The scheme can be seen in *Figure 1.3b*.

The ammonia created enters the SCR-catalyst where it is adsorbed and can react as described in the next section.



(a) Flow chart for determination of droplet–wall interaction from [13].



(b) The different regimes of droplet–wall interactions from [17].

Figure 1.3: Two proposed schemes to determine the droplet–wall interaction.



As European legislation Euro V was introduced, it made it necessary for Scania to implement urea-SCR. Today, urea-SCR without EGR is most commonly used as it has several advantages over the combined technology. Without EGR, the engine is lighter, smaller and has a better fuel economy. Engines without EGR are therefore cheaper to manufacture and to operate.

### 1.3.2 Hydrocarbon Selective Catalytic Reduction

Hydrocarbon Selective Catalytic Reduction (HC-SCR) reduces  $\text{NO}_x$  by reacting them with either remaining hydrocarbons in the exhaust and/or injected hydrocarbons, depending on the amount of unburned hydrocarbons in the exhaust. In theory, diesel can be used as the hydrocarbon which would eliminate the need for an additional reducing agent. Injecting diesel would however affect the fuel economy since it utilizes the fuel for  $\text{NO}_x$  reduction instead of for propelling the truck.

More research is needed before this technology can compete with urea-SCR. The activity of the proposed catalysts are not high enough in a wide enough temperature window. Small amounts of added hydrogen to the exhaust increase the activity but requires a hydrogen tank on-board or a hydrogen generating system [21].

### 1.3.3 Lean $\text{NO}_x$ Trap

A catalyst able to store  $\text{NO}_x$  under lean conditions and reducing it under rich conditions has been developed. There are three active components in the catalyst's washcoat [22]

- An oxidation catalyst (Pt)
- An adsorber (alkaline metal oxide, e.g. BaO)
- A reduction catalyst (Rh)

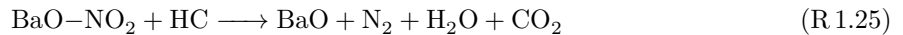
Under lean conditions, NO is first oxidized by oxygen over the Pt-catalyst



after which the  $\text{NO}_2$  is adsorbed onto the adsorber



After a certain amount of time, the trap reaches its maximum capacity and rich conditions are needed to regenerate the trap. This is done either by injecting hydrocarbons into the exhausts or by engine control.  $\text{NO}_2$  is released from the adsorber and reacts together with hydrocarbons over the Rh-catalyst.



Sulfur readily adsorbs into the alkaline metal oxide and poisons the structure, and unlike  $\text{NO}_2$ , sulfur oxides bind strongly to the adsorber and no good strategy to regenerate the trap has been developed yet. This and the fact that the fuel economy is worsened by the rich conditions during trap regeneration have prevented this technique from being implemented as a de $\text{NO}_x$  strategy for trucks [22].

## 1.4 Heat Transfer Theory

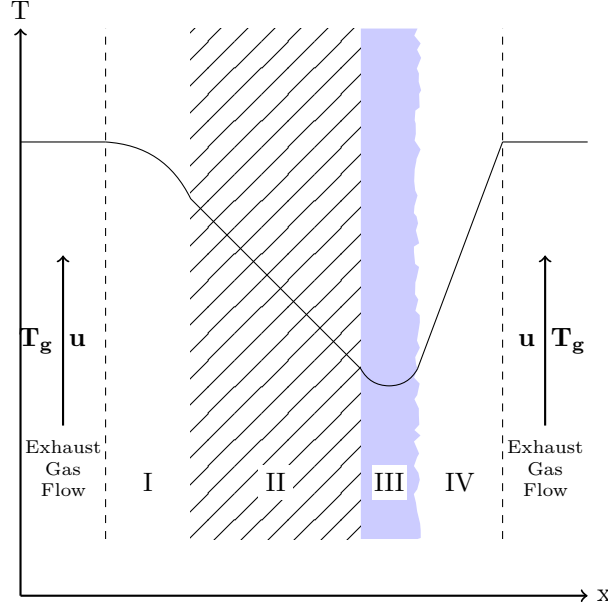


Figure 1.5: Sketch of the temperature profile over a wall where urea droplets have formed a film.

In *Figure 1.5*, four zones are marked. The heat transfer in these zones can be modeled as differential equations. In general they have the form:

$$\underbrace{\rho c_p \frac{\partial T}{\partial t}}_{\text{Accumulation}} = \underbrace{k \nabla^2 T}_{\text{Conduction}} - \underbrace{\rho c_p u \nabla T}_{\text{Convection}} + \underbrace{Q_G}_{\text{Production}} \quad (1.7)$$

The parameters are explained in *Table 1.3*.

Table 1.3: Parameter explanations for partial differential equation

Parameters	Explanation	Unit
$\rho$	Density of fluid	$\text{kg m}^{-3}$
$c_p$	Specific heat of fluid	$\text{J kg}^{-1} \text{K}^{-1}$
$k$	Thermal conductivity of fluid	$\text{W m}^{-1} \text{K}^{-1}$
$u$	Velocity of fluid	$\text{m s}^{-1}$
$Q_G$	Heat production	$\text{J m}^{-3} \text{s}^{-1}$

In the marked zones, the bulk velocity is zero and therefore the second term in the right-hand-side of *Equation (1.7)* disappears. The production term is non-zero in zone III since energy is used for the evaporation of water and urea. This can be seen as a negative production. *Equation (1.7)* becomes

$$\rho c_p \frac{\partial T}{\partial t} = k \nabla^2 T + Q_G \quad (1.8)$$

Different zones will have different governing differential equations. They will be coupled through the boundary conditions, which preserves the heat fluxes through the boundary. The flux,  $q$  can be written:  $q = -k \nabla T$  when heat is transferred by conduction and  $q = h \Delta T$  when heat is transferred by convection.  $h$  is a heat transfer coefficient,  $h = k/\Delta x$  [ $\text{W K}^{-1} \text{m}^{-2}$ ]. For the interface between phase I and II, this means that

$$h_I \Delta T_I = k_{II} \nabla T_{II} \quad (1.9)$$

And similar for the other interfaces.

In phase I and IV, the heat transfer can be dealt with using empirical correlations. In phase IV, the flux of urea droplets also have to be considered as a contributor to the energy balance. The energy balance in phase III will need to take into account both the heat used for evaporation of water and the heat used for evaporation of urea. This will depend on the flux of urea droplets.

## 1.5 Previous Research and Experiments

In this section, others experiments and the ones planned in this thesis will be described.

### 1.5.1 Previous Test Rigs

#### 1.5.1.1 Rigs at Scania

**Asgari [23]** built a rig for tests on urea evaporation at Scania in 2010. In this thesis, the same facility, Aftertreatment Rig 1 (AR1) for controlling gas flow, gas temperature and more will be used. The part where urea is injected and evaporated will have a new design to give it the desired properties. Asgari did experiments both with an optical rig and with a non-optical rig. The temperature was measured with thermocouples and gas composition measured with Fourier Transform Infrared spectroscopy (FTIR). Both rigs had a cylindrical shape and were made of stainless steel. The optical rig had its shell partly cut out and replaced with glass to allow visual inspection.

The aim with the optical rig was to see how the temperature varied along the cylinder in order to calculate the evaporation rate. However there were some problems with putting the thermocouples in the right place (at the location of the film) and therefore reliable calculations could not be made.

**Rapp [24]** studied the evaporation process in a real aftertreatment system using FTIR. Gas was sampled for FTIR analysis at three different points and at the same points, temperatures were measured. Rapp assumed that all urea evaporated and underwent thermolysis, and by measuring the concentrations at different positions, assuming first order kinetics and assuming that the exhaust pipe behaves like a plug flow reactor, Rapp [24] was able to estimate the kinetic constants.

**Wedlund [25]** studied the influence of spray parameters such as dosing unit pressure, spray angle and dosing frequency. Experiments were done in AR1 in a cylindrical exhaust pipe. Temperatures were measured with thermocouples and concentration of ammonia was measured with FTIR. Besides from having thermocouples outside of the pipe, the temperature was measured inside the pipe with flow intercepting thermocouples. Film formation could be observed on the thermocouples inside the pipe as local cold spots was observed under certain conditions.

#### 1.5.1.2 Rigs in the Literature

**Tang et al. [6]** built a test rig with a glass-pipe in which the urea solution was injected, using an air-assisted injector. The outlet gas was analyzed with FTIR and the formed deposits with Thermogravimetric Analysis (TGA) and Differential Scanning Calorimetry (DSC). The aim of their study was to investigate the deposit chemistry and not to investigate when and how films were formed. They did however develop a model to calculate the film thickness and temperature but no validation of the model was presented.

**Grout et al. [12]** also experimented on the evaporation of urea solution and analyzed the film and droplets with a normal camera and Laser light Sheet Imaging (LSI). A glass pipe was used and underneath the pipe and paper with a pattern was placed so that the camera would have something to focus on. When a film was formed, the pattern would be deformed due to diffraction in the liquid.

The droplet distribution in the pipe was determined with LSI. By shining a laser wall through the pipe and recording the scattered light at a specific angle towards the laser wall, the droplet distribution could be calculated.

The aim of their study was to develop a methodology for studying the droplet evaporation and film formation.

**Schulz et al. [16]** studied the fuel injection by injecting a fuel spray onto a heated plate while monitoring the plate temperature with an Infrared (IR)-camera from underneath. The parameters of interest in the study was initial plate temperature, spray angle, distance between injector and plate and injector pressure. They created a model to calculate the temperatures and heat fluxes through the plate.

The plate was heated electrically by sending a known current through the high resistance plate and the surroundings were at room temperature. This study will be done under more realistic conditions, but the conditions will in return not be as controlled.

## 1.6 Motivation

Heavy-duty trucks under light load have problems with the evaporation of AdBlue<sup>®</sup>. The exhaust gases sometimes have a too low temperature for efficient evaporation of all the injected urea. Instead, the urea solution forms liquid films on the exhaust pipe walls. Inside the films, undesired reactions take place and this can lead to the formation of deposits. The deposits may increase the pressure drop over the muffler and give another stoichiometry as the gases enter the SCR, potentially leading to NH<sub>3</sub> emissions.

This thesis will examine the evaporation process and investigate how films are formed to determine how the formation of wall films can be minimized.

## 1.7 Aims and Goals

A test rig will be built in which gas flow, gas temperature, AdBlue<sup>®</sup> and plate properties will be controlled. Urea solution will be injected into a hot air stream and hit a plate whose temperature is monitored with an IR-camera and thermocouples. Urea will be injected with a constant dosing rate until steady state is reached, with or without a formed film. If no film is created, the dosing rate will be increased and the experiment repeated. When the maximum dosing rate per unit time has been determined, this quantity can be plotted against the energy content of the gas phase, expressed as J s<sup>-1</sup> and a model can be developed for determining the maximum allowed dosing rate before a film is formed. A maximum dosing rate at different conditions can be used to prevent film formation and hence also to prevent NO<sub>x</sub> emissions and NH<sub>3</sub>-emissions.

# Chapter 2

## Experiments

### 2.1 Experimental Design

This section will describe the design of the experiments.

#### 2.1.1 Desired Properties of the Test Rig

Since the goal is to examine and understand the film and deposit formation, the test rig should be designed to enable this. It should provide an environment where experiments can be done while important parameters are controlled and the results recorded. Important parameters are gas temperature, gas flow rate, gas composition, spray angle, urea dosage rate, plate angle against gas flow, plate thickness and distance between injector and plate.

Both visual and IR observations will be done. An IR-camera will be used to follow the film formation process. The injected spray will cool the plate allowing observations with the infrared camera. An IR-camera can only see through materials transparent to infrared light. Most solid materials are not transparent in this electromagnetic region so a glass made of a special material has to be used to allow for observations using the IR-camera. The material also need to be able to withstand the high temperatures of the test rig.

Observations with the IR-camera should be possible to do both from the top side and the bottom side of the test rig. Therefore, the rig should have IR transparent windows both on the top and on the bottom.

Visual observation is also desired so the rig should have normal glass that can withstand high temperature on one side.

To be able to vary plate properties such as plate angle against gas flow, plate thickness and plate height, the plate needs to be replaceable and thus cannot be welded directly into the test rig. It must also be possible to open the test rig, so that the plate can be adjusted. Thermocouples will be attached to the plate so that the IR-camera can be calibrated against a known temperature.

#### 2.1.2 Test Rig Design

Earlier test rigs at Scania have not had the same area of focus and therefore this test rig needs a novel design. From the desired properties, the design in *Figure 2.1* was suggested.

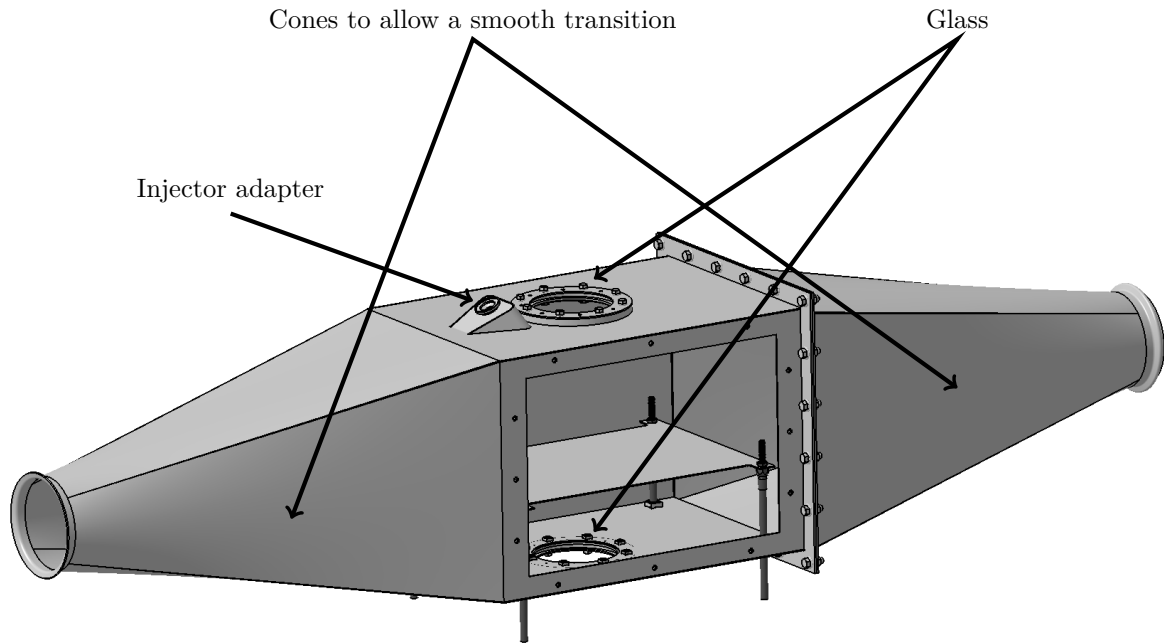


Figure 2.1: Image depicting the test rig in the blueprints for the rig.

This design has the flexibility needed. The manufactured test rig is shown in *Figure 2.2*.

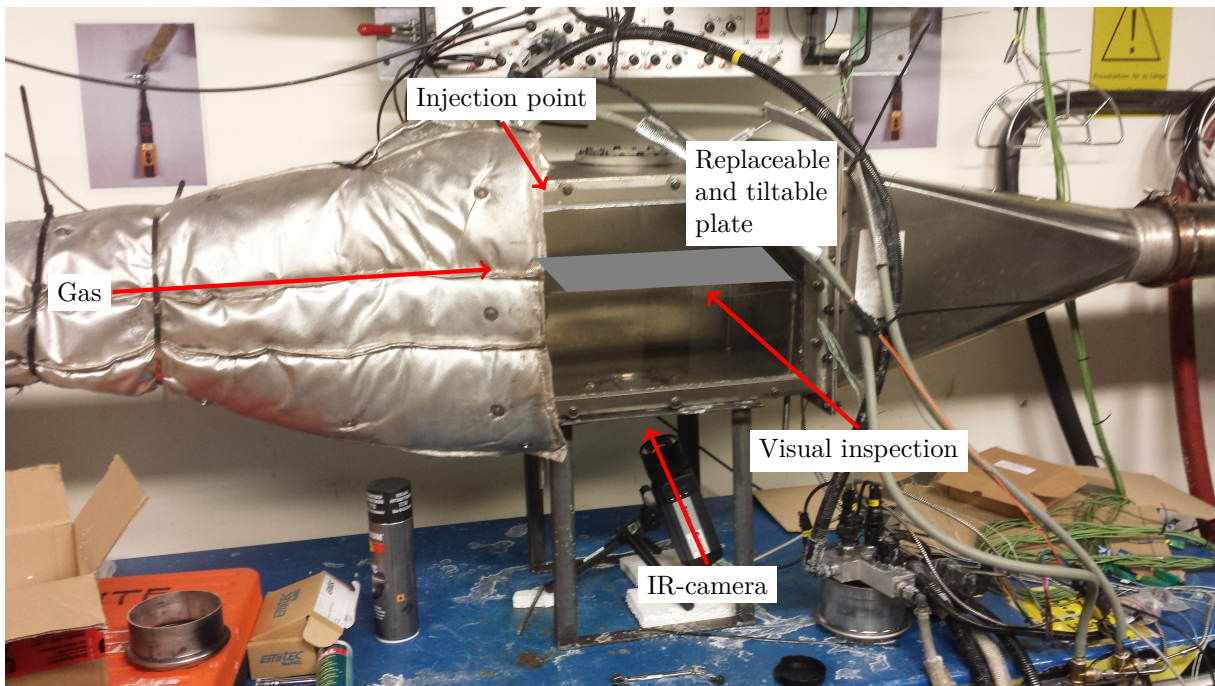


Figure 2.2: Photo of the finished test rig.

## 2.2 Experimental Setup

The experiments were done in AR1, a hot gas test cell at Scania. Programming of test sequences were done in Scania Testbed Platform (STP), a system developed and maintained by Scania.

Two types of experiments were done. One kind where the film area and temperature drop ( $\Delta T$ ) were measured for different conditions and then one kind where the deposit formation over a longer time period

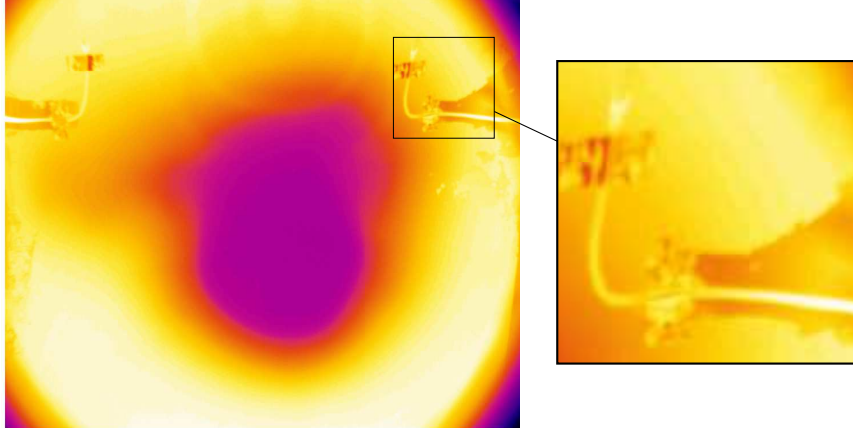


Figure 2.3: IR-camera photo with magnification showing the thermocouple threads used for pixel-length calibration.

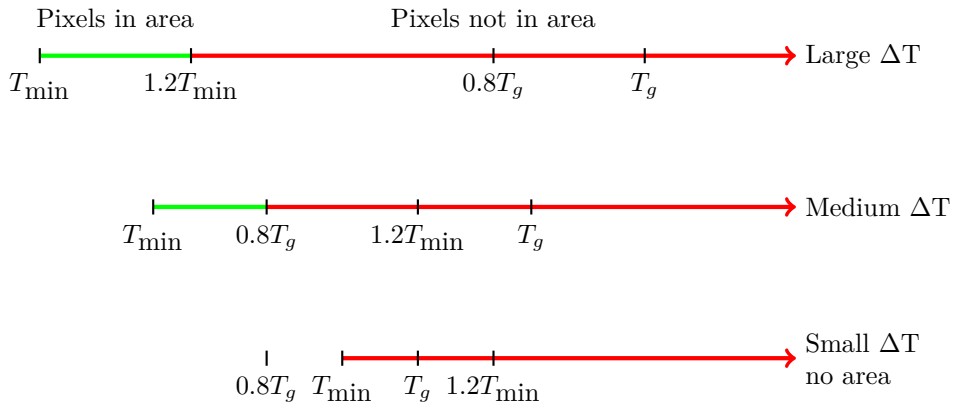


Figure 2.4: Temperature axis showing which pixels that were counted in the area calculation.

was investigated, in this kind of experiments visual observations were more important than in the first kind.

The first kind of experiment is hereafter referred to as *dosing stairs* and the second kind of experiment is hereafter referred to as *long runs*.

During the dosing steps, the dosage was kept constant for 10 minutes and after some time, steady state was reached and the temperature drop and area was recorded. To get the area, the number of pixels fulfilling two conditions were counted and multiplied with a proportionality constant to change from pixels to  $\text{cm}^2$ . This proportionality constant was found through repeated measurements of the width of the thermocouples thread in the IR-camera photos. An example photo is seen in *Figure 2.3*, where the thermocouples are seen as white threads. Since the width of these threads is known, this made it possible to correlate pixels to area. The average constant was  $45 \text{ px cm}^{-1}$ .

The two conditions determining the area were:

- $T \leq 1.2T_{\min}$
- $T < 0.8T_g$

It can be illustrated on an axis as in *Figure 2.4*. Measurements indicating  $0 \text{ cm}^2$  therefore has no pixels fulfilling  $T < 0.8T_g$  and  $T \leq 1.2T_{\min}$ , as in the third line in *Figure 2.4*.

The dosage was varied in the region  $0\text{--}80 \text{ g min}^{-1}$  (lower max level for lower gas temperatures), and the increment was typically  $10 \text{ g min}^{-1}$ . For these experiments, the gas flow rate and gas temperature was varied in the ranges  $400\text{--}1200 \text{ kg h}^{-1}$  and  $200\text{--}400 \text{ }^\circ\text{C}$  respectively. The points at which the dosing steps were done can be seen in *Figure 2.7*.

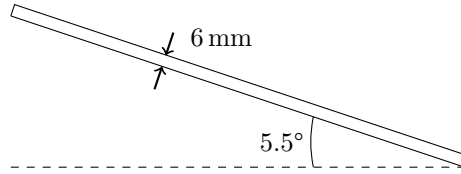


Figure 2.5: Schematic picture with the dimensions of the tilted thick plate.

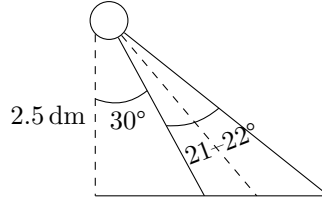


Figure 2.6: Schematics of the Injector and Plate Geometry

In the long runs, the dosing was kept at a level high enough so that a wall film and deposits would be formed. This level was found through experiences from the dosing step experiments.

So far, only variation of gas properties has been described. The plate thickness and plate angle was also varied and the same experimental matrix as in *Figure 2.7* used. This means that the experiments described earlier were done three times, once for a thin plate, once for a thick plate and once for a thick tilted plate. All plates were made of stainless steel, the thin plate had a thickness of 1.5 mm while the thick plate had a thickness of 6 mm. The tilted plate was tilted  $5.5^\circ$  as in *Figure 2.5*. Tilting the plate more was impossible due to deformation of the test rig. The relatively thin plate deformed when exposed to the high welding temperatures.

### 2.2.1 The Injector

Injection was done from the top of the test rig, at the position depicted in *Figure 2.2*. More information on the geometry can be seen in *Figure 2.6*

### 2.2.2 The Infrared Camera

The IR-camera used is a FLIR SC665 camera. It comes with a user friendly Graphical User Interface (GUI) but also has LabVIEW drivers. It can be connected to the computer with an Ethernet cable or an USB-cable, but the Ethernet interface allows for significantly higher communication speeds. The camera also has digital I/O contacts which makes it possible to send or receive electrical signals to the camera.

At first, the intention was to use the LabVIEW drivers to connect the camera to the control program and control both the test rig and the camera from one computer. This would have been the most convenient solution but also time consuming. After discussion with technical support from the camera company, this solution was discarded in favor of using the GUI from the camera. Due to the LabVIEW drivers being outdated and the time limit of the thesis.

In the end, the camera was connected with an Ethernet cable to a laptop onto which all data was stored while the camera was controlled through the digital I/O.

When measuring the temperature of a surface, it is important to know its emissivity. Surfaces with less emissivity look colder compared to hot surfaces since less heat is radiated from the surface. In the earliest experiments, the plate surface was observed *as is* with the IR-camera. Due to the steel surface reflecting much of the infrared light, reflections disturbed the measurements. To solve this, the bottom side of the plates were sprayed with a black paint which eliminated the reflections.

With the camera GUI, the emissivity was calculated using the measured temperatures from the thermocouples attached to the plate. After many measurements, a value of 0.74 was taken to be the average of

the emissivity of the steel surface.

Measurements were exported from the camera GUI into MATLAB in which all calculations were made.

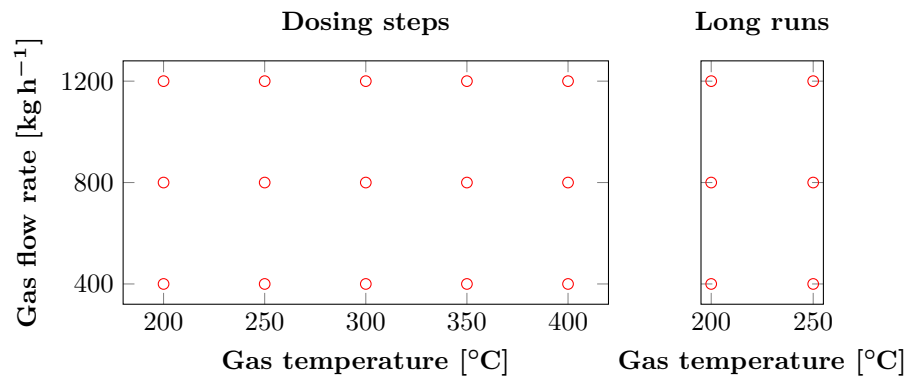


Figure 2.7: Points at which experiments are done.

## Chapter 3

# Results and Discussion

After collecting all the experimental data, the influence of plate properties and gas properties on the temperature drop and film area was investigated. The effect on the temperature drop and film area can be seen in *Figures 3.1 and 3.2*

### 3.1 Influence of Plate Properties on Evaporation Performance

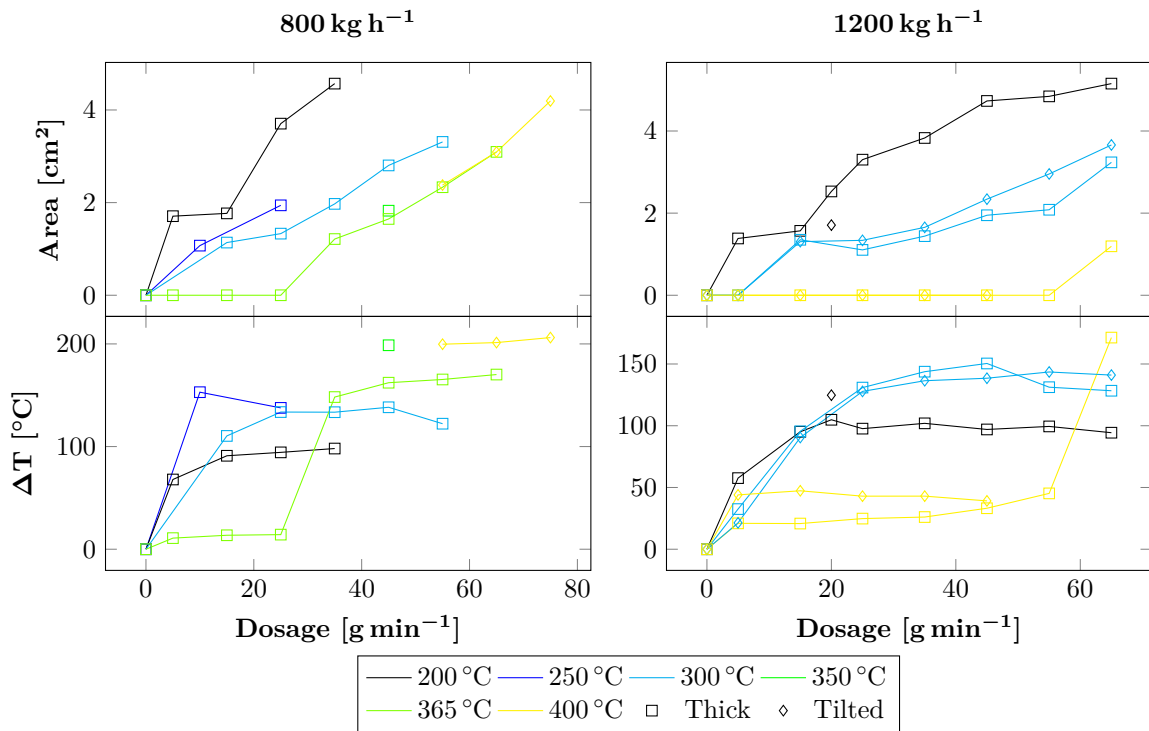


Figure 3.1: Temperature drop and area measurements for a thick and a tilted thick plate at  $800 \text{ kg h}^{-1}$  and  $1200 \text{ kg h}^{-1}$

#### 3.1.1 Effect of Tilting Plate

Tilting the plate to  $5.5^{\circ}$  did not have a big effect on the temperature drop and area. In fact, the tilted plate even have a slightly higher wetted area than the none-tilted plate as can be seen for the  $1200 \text{ kg h}^{-1}$ ,  $300^{\circ}\text{C}$  curve in *Figure 3.1*.

Note that two different behaviors for the curves are seen in *Figure 3.1*. Up to 300 °C, the temperature drop curves follow an increasing exponential decay while the curves at 365 °C and above a behavior that is better described as a sigmoid curve.

Since no pattern is observed, measurements for the thick and tilted thick plate are shown as one in the following figures.

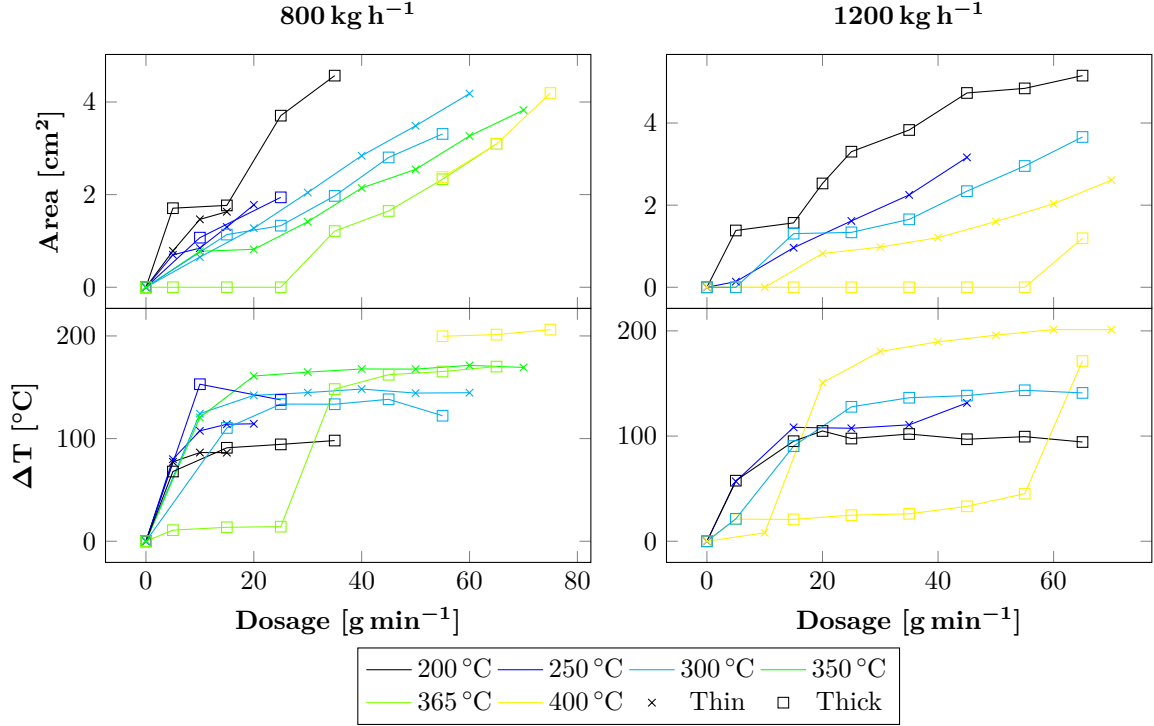


Figure 3.2: Temperature drop and area measurements for a thin and a thick plate at 800 kg h<sup>-1</sup> and 1200 kg h<sup>-1</sup>

### 3.1.2 Effect of Changing Thickness of Plate

*Figure 3.2* shows the area and temperature drop for thin and thick plates with 800 kg h<sup>-1</sup> and 1200 kg h<sup>-1</sup>.

At lower dosages for temperatures up to 300 °C, it is hard to distinguish any clear trends but at higher dosages, the thicker plate has a smaller temperature drop and a smaller area. At 365 °C and 400 °C, the thick plate is almost unaffected by the dosing up to 25 g min<sup>-1</sup> and 55 g min<sup>-1</sup>, respectively. At higher dosages than these, the temperature drop and measured area is almost as high as for the thinner plate though.

## 3.2 Influence of Gas Flow on Evaporation Performance

From the 250 °C-graphs in *Figure 3.3*, changing the gas flow rate seem to have a small beneficial effect on the temperature drop and area. However, the 300 °C does not show the same, clear, trend. In those two graphs, the curves overlap and no clear effect on the temperature drop and area is seen.

At dosages in the range 5–20 g min<sup>-1</sup>, the observed area is fairly constant. As the dosage is increased further, the area increases linearly. From visual inspection, it looks like this is a region where a film is not yet formed, but the surface of the plate is wet. Every time the spray hits, the area increases some and then shrinks, until the spray hits again. The observed constant area in this region therefore corresponds to the area directly hit by the spray.

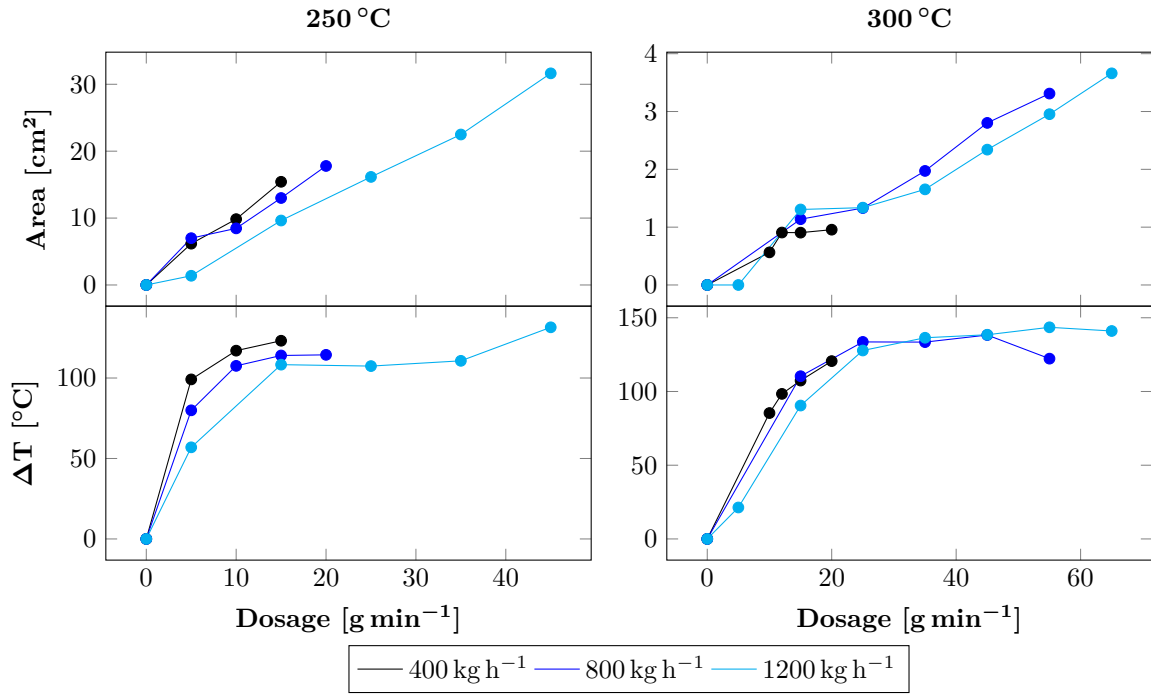


Figure 3.3: Temperature drop and area measurements at different gas flow rates for 250 °C and 300 °C

### 3.3 Influence of Gas Temperature on Evaporation Performance

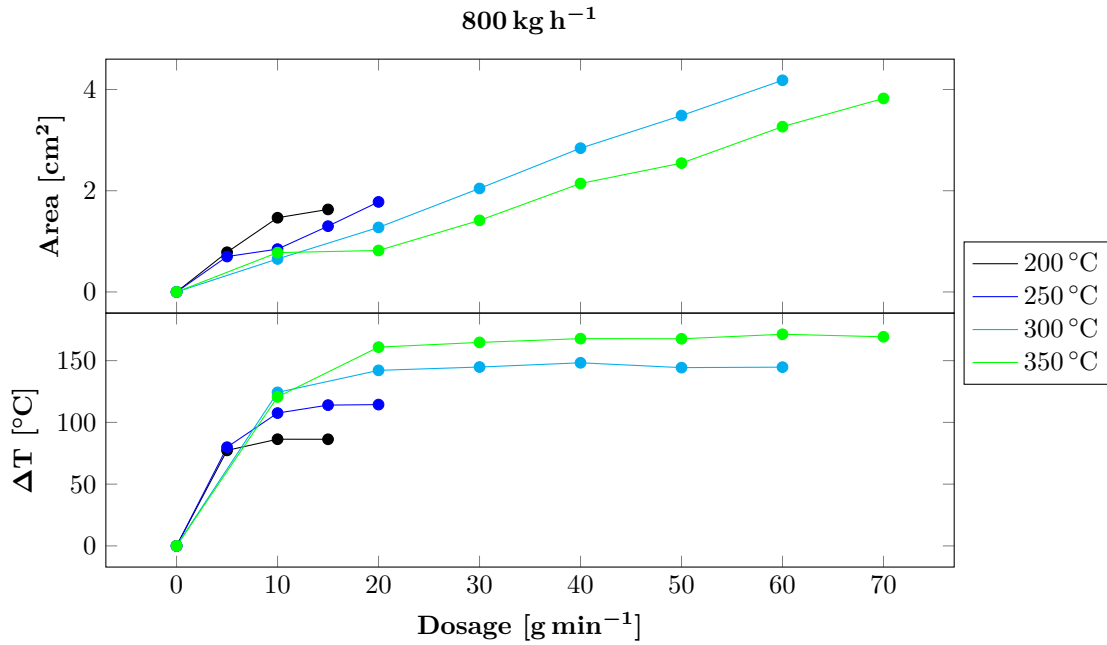


Figure 3.4: Temperature drop and area measurements at different gas temperatures for 800 °C

Changing the temperature has a big effect on the temperature drop and area. Unlike in *Figure 3.3*, the curves are clearly separate of each other and smaller temperature drops and areas are observed as the temperature increases.

For the temperature drops, the curves increase like an exponential decaying function to a constant value

depending on gas temperature.

### 3.4 Instantaneous Evaporation

By looking more closely on the temperature profiles of the plates during the dosing steps, the phenomena with an unaffected plate can be better understood. *Figures 3.5 and 3.6* shows the temperature curve during the 10 min that the dosing is active.

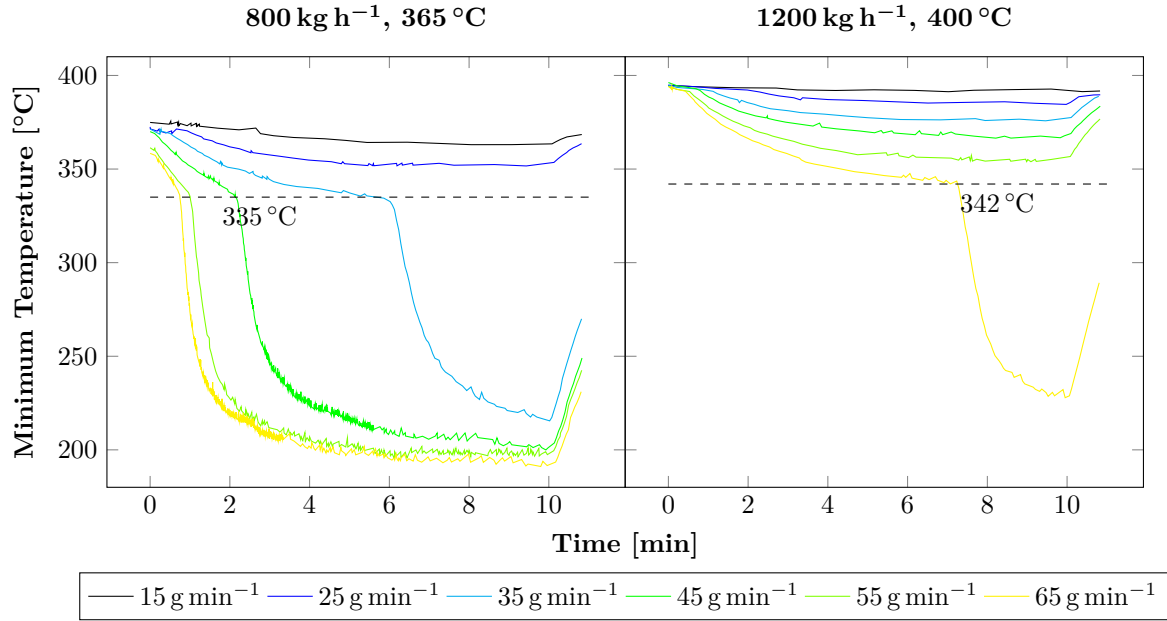


Figure 3.5: The minimum measured temperature for thick plates during the dosing steps. The sudden plunge in temperature happens at almost the same minimum temperature for all curves.

There is a very clear critical temperature below which the minimum temperature plunges for the thicker plate. For the thinner plate in *Figure 3.6*, the drop happens at lower dosing and the exact temperature where this happens is not as clear.

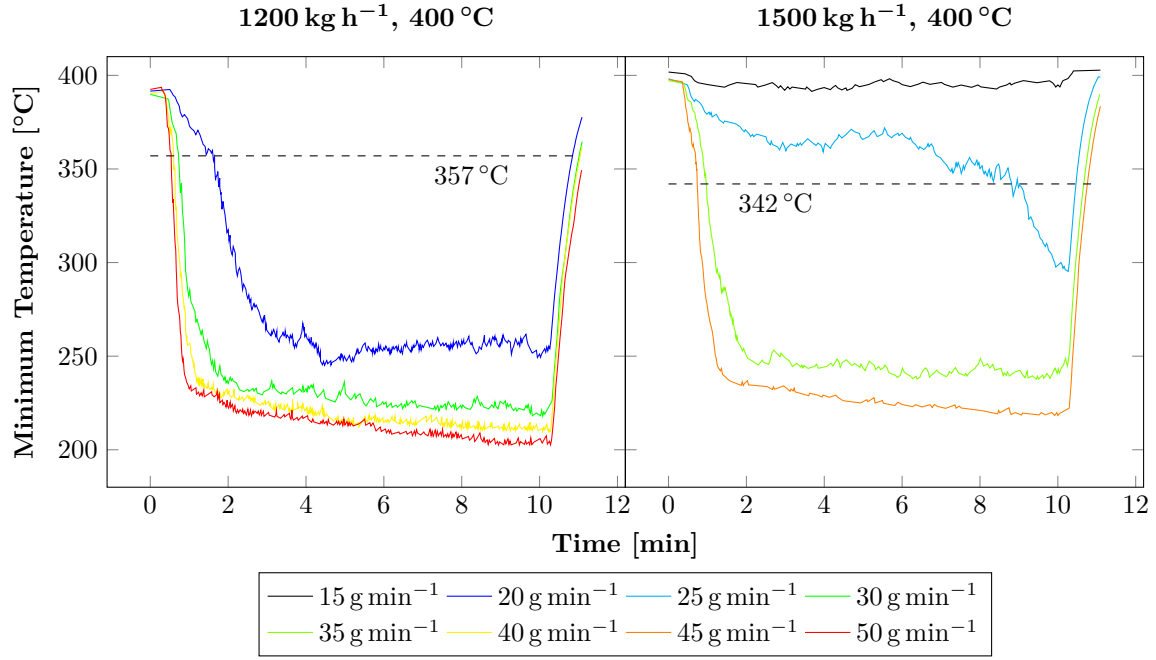


Figure 3.6: The minimum measured temperature for thin plates during the dosing steps. The sudden plunge in temperature happens at a temperature pretty close to the temperature for thicker plates.

To summarize, the found critical temperatures are collected in *Table 3.1*.

Table 3.1: Measured critical temperature for different plates and conditions

Plate	Gas flow rate [kg h <sup>-1</sup> ]	Gas temperature [°C]	Critical temperature [°C]
Thick	800	365	335
Thick	800	400	342
Tilted	1200	400	335
Thin	1200	400	357
Thin	1500	400	342

Not all measurements gave temperature profiles with distinguishable critical temperatures, which is why *Table 3.1* does not contain more entries.

### 3.5 Temperature Recovery of the Plates

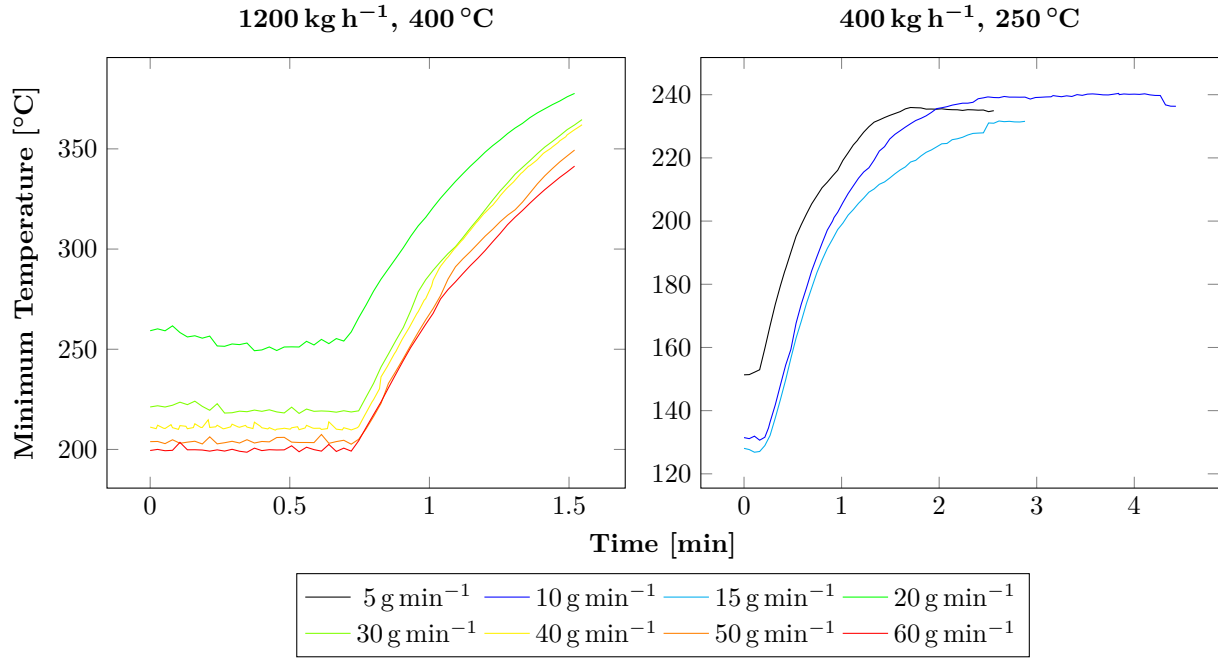
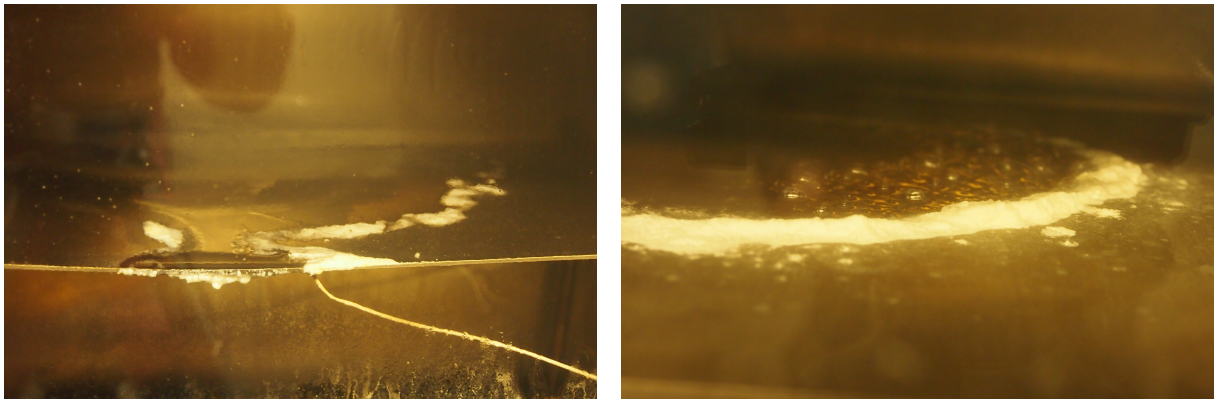


Figure 3.7: The minimum temperature profile after the dosing ends for two experiments

Since AdBlue® contains both water and urea and water and the latter compound has a higher vapor pressure than urea, it has been hypothesized that film evaporation happens in two distinct steps. First, all or almost all water is evaporated, then urea is evaporated. This would mean that the recovery profile for the plates should contain two regions with different slopes. However, as can be seen in *Figure 3.7*, this is not observed. The curves in the figure look smooth. It might be because the wall film is thin. A thin wall film gives a fast heating phenomena and differences in slope might be lost in the disturbances.

### 3.6 Deposit Formation at Different Temperatures



(a) Typical wall film and deposit process at lower temperatures. In this case after 2 h of constant dosing.

(b) Typical wall film and deposit process at higher temperatures. In this case after 30 min of constant dosing

In the longer runs, the deposit formation was compared at low and high temperature conditions. At lower temperatures, the film tended to spread out over a large area while at higher temperature, the deposits formed quickly at the edge of the spray impact area and hindered further expansion of the film.

In *Figures 3.8a* and *3.8b*, typical wall film and deposit behavior is seen. In *Figure 3.8a*, the lower temperature behavior is seen. The film has spread out over a large area and not much deposits are formed, instead a wall film covering a very large area is seen.

At higher temperatures, the opposite case is observed. The wall film is relatively small and deposits build up fairly quickly at the film edge, as seen in *Figure 3.8b*.

# Chapter 4

## Conclusions

The conclusions are:

- Much can be learned about urea evaporation by using a simplified test rig like the one used in this thesis. Furthermore, an infrared camera is useful for determining temperature drops as it measures the temperature of an area and not a point.
- There is a region at lower dosages and low gas temperatures where the measured area is constant. The measured area in this region corresponds to the spray impact area and the observed film is very thin.
- If dosing is further increased, the film gains height and start spreading out. A linear increase of the area is observed as the dosage is increased.
- At plate temperatures above 340 °C, the AdBlue<sup>®</sup> evaporates quickly to a urea dust. This has little effect on the plate, it is cooled slowly. As the plate reaches 340 °C the cooling is enhanced and the temperature drops rapidly.
- Thick plates handles moderate dosages better than thin plates, but after a certain dosage, depending on gas properties, the performance is about the same. This is due to losing the ability of turning the AdBlue<sup>®</sup> into a urea dust.
- At higher gas temperatures ( $\gtrsim 350$  °C), deposits fairly quickly build up at edge of spray impact area.
- At lower temperatures a film is instead formed, which spreads out and forms thin deposits. Larger deposits form at obstacles and with time at film edge.

### 4.1 Recommendations for Future Work

- Improve test rig to make it possible to study the spatial temperature variation to where deposits are formed. Using the IR-camera from the top side of the plate would also be interesting, as well as varying the plate properties more.
- Improve light in test rig to be able to get better photos of the process and enable automatic photo shootings of the process.

A few drawbacks with the used test rig design:

- The thin steel used made the rig deform when exposed to heat (during welding)
- It was quite time consuming to replace the plate due to the big side window consisting of an inner and outer frame and graphite gaskets that were only connected to each other by the screws that attached the window to the rig. When detached, the parts fell apart and had to carefully be reassembled
- If the rig would have handles to which the test cells' overhead (bridge) crane can be attached, it would make the testing more flexible



# Acronyms

**$\Delta T$**  temperature drop.

**AdBlue<sup>®</sup>** Urea–water solution containing 32.5 % urea and 67.5 % deionized water.

**AR1** Aftertreatment Rig 1.

**CYA** Cyanuric Acid.

**DOC** Diesel Oxidation Catalyst.

**DSC** Differential Scanning Calorimetry.

**ECU** Electrical Control Unit.

**EGR** Exhaust Gas Recirculation.

**FTIR** Fourier Transform Infrared spectroscopy.

**GUI** Graphical User Interface.

**HC-SCR** Hydrocarbon Selective Catalytic Reduction.

**IR** Infrared.

**LNC** Lean NO<sub>x</sub> Catalyst.

**LSI** Laser light Sheet Imaging.

**NO<sub>x</sub>** Nitrogen Oxides.

**PM** Particulate Matter.

**SCR** Selective Catalytic Reduction.

**STP** Scania Testbed Platform.

**TGA** Thermogravimetric Analysis.

**UDS** Urea Dosing System.

**WHSC** World Harmonized Stationary Cycle.

**WHTC** World Harmonized Transient Cycle.

# List of Symbols

$A_{\square}$  Area of region indicated by subscripts.

$Ca$  Capillary number.

$d$  Diameter of droplet.

$g$  gravitational acceleration constant.

$h$  Heat transfer coefficient.

$K$  Parameter used in the analysis of droplet wall interactions.

$m_a$  Mass of droplets leaving a surface.

$m_b$  Mass of droplets hitting a surface.

$M_w$  Molar mass.

$\nabla$  Spatial derivative, in three dimensions  $\nabla = (\frac{\partial}{\partial x}, \frac{\partial}{\partial y}, \frac{\partial}{\partial z})$ .

$Oh$  The Ohnesorge number, represents fluid properties.

$Re$  The Reynolds number, the ratio between inertial forces and viscous forces.

$\rho_{\square}$  Density in region indicated by subscript.

$\sigma$  Surface tension.

$T_{\square}$  Temperature in region indicated by subscript.

$T_L$  Leidenfrost temperature, temperature at which the rate of evaporation of a droplet is at a local minimum.

$T_{vap}$  Boiling temperature.

$We$  The Weber number, the ratio between inertial forces and surface tension forces.

# Subscripts

$\square_b$  In bulk (of gas phase).

$\square_d$  In urea solution.

$\square_g$  In gas phase.

$\square_{imp}$  In impacting urea solution.

$\square_s$  At surface.

$\square_w$  In plate.

# Bibliography

- [1] Heavy-duty truck and bus engines, September 2012. URL <http://www.dieselnet.com/standards/eu/hd.php>.
- [2] Mellor, A. M., Mello, J. P., Duffy, K. P., Easley, W. L., and Faulkner, J. C. Skeletal mechanism for nox chemistry in diesel engines. In *SAE Technical Paper*. SAE International, 05 1998. doi: 10.4271/981450.
- [3] Khair, M. K. and Jääskeläinen, H. Emission formation in diesel engines, November 2008. URL [http://www.dieselnet.com/tech/diesel\\_emiform.php](http://www.dieselnet.com/tech/diesel_emiform.php).
- [4] Glarborg, P., Johnsson, J. E., and Dam-Johansen, K. Kinetics of homogeneous nitrous oxide decomposition. *Combust. Flame*, 99(3-4):523–532, December 1994. doi: 10.1016/0010-2180(94)90045-0.
- [5] Sebelius, S., Le, T., Pettersson, L., and Lind, H. Identification of urea decomposition from an SCR perspective; a combination of experimental work and molecular modeling. *Chem. Eng. J.*, 231: 220–226, September 2013. doi: 10.1016/j.cej.2013.06.124.
- [6] Tang, T., Zhang, J., Jin Shuai, S., and Cao, D. Urea decomposition at low temperature in SCR systems for diesel engines. In *SAE Technical Paper*. SAE International, 10 2014. doi: 10.4271/2014-01-2808.
- [7] Majewski, W. A. Selective catalytic reduction, May 2005. URL [http://www.dieselnet.com/tech/cat\\_scr.php](http://www.dieselnet.com/tech/cat_scr.php).
- [8] Ebrahimian, V., Nicolle, A., and Habchi, C. Detailed modeling of the evaporation and thermal decomposition of urea-water solution in scr systems. *AIChE J.*, 58(7):1998–2009, July 2012. doi: 10.1002/aic.12736.
- [9] Schaber, P., Colson, J., Higgins, S., Thielen, D., Anspach, B., and Brauer, J. Thermal decomposition (pyrolysis) of urea in an open reaction vessel. *Thermochim. Acta*, 424(1-2):131–142, December 2004. doi: 10.1016/j.tca.2004.05.018.
- [10] Chen, Z.-c., Yang, W.-j., Zhou, J.-h., LV, H.-k., Liu, J.-z., and Cen, K.-f. H<sub>2</sub>O hydrolysis performance in urea-water solution thermohydrolysis process with and without catalysts. *J. Zhejiang Univ. Sci. A*, 11(11):849–856, November 2010. doi: 10.1631/jzus.A0900798.
- [11] Yim, S., Kim, S., Baik, J., and Nam, I. Decomposition of urea into NH<sub>3</sub> for the SCR process. *Ind. Eng. Chem. Res.*, 43(16):4856–4863, 2004. doi: 10.1021/ie034052j.
- [12] Grout, S., Blaisot, J., Pajot, K., and Osbat, G. Experimental investigation on the injection of an urea-water solution in hot air stream for the SCR application: Evaporation and spray/wall interaction. *Fuel*, 106:166–177, 2013. doi: 10.1016/j.fuel.2012.09.022.
- [13] Chen, C., Amlee, D. R., Johns, R. J. R., and Zeng, Y. Detailed modeling of liquid fuel sprays in one-dimensional gas flow simulation. In *SAE Technical Paper*. SAE International, 10 2004. doi: 10.4271/2004-01-3000.
- [14] Moreira, A. *Handbook of Atomization and Sprays*. Springer Science+Business Media, 2011. doi: 10.1007/978-1-4419-7264-4\_21.
- [15] Mundo, C., Sommerfeld, M., and Tropea, C. Droplet-wall collisions: Experimental studies of the deformation and breakup process. *Int. J. Multiphase Flow*, 21(2):151–173, 03 1995. doi: 10.1016/0301-9322(94)00069-V.

- [16] Schulz, F., Schmidt, J., Kufferath, A., and Samenfink, W. Gasoline wall films and spray/wall interaction analyzed by infrared thermography. *SAE Int. J. Engines*, 7(3):1165–1177, 04 2014. doi: 10.4271/2014-01-1446.
- [17] Birkhold, F., Meingast, U., Wassermann, P., and Deutschmann, O. Analysis of the injection of urea-water-solution for automotive scr denox-systems: Modeling of two-phase flow and spray/wall-interaction. In *SAE Technical Paper*. SAE International, 04 2006. doi: 10.4271/2006-01-0643.
- [18] Kuhnke, D. *Spray/Wall-Interaction Modelling by Dimensionless Data Analysis*. PhD thesis, Technischen Universität Darmstadt, 2004.
- [19] Squaiella, L., Martins, C., and Lacava, P. Strategies for emission control in diesel engine to meet euro vi. *Fuel*, 104:183–193, 03 2013. doi: 10.1016/j.fuel.2012.07.027.
- [20] Khair, M. K. and Jääskeläinen, H. Exhaust gas recirculation, September 2014. URL [http://www.dieselnets.com/tech/engine\\_egr.php](http://www.dieselnets.com/tech/engine_egr.php).
- [21] Chaieb, T., Delannoy, L., Casale, S., Louis, C., and Thomas, C. Evidence for an H<sub>2</sub> promoting effect in the selective catalytic reduction of NO<sub>x</sub> by propene on Au/Al<sub>2</sub>O<sub>3</sub>. *Chem. Commun.*, 51(4): 796–799, 2015. doi: 10.1039/C4CC07349E.
- [22] Heck, R. M., Farrauto, R. J., and Gulati, S. T. *Catalytic Air Pollution Control Commercial Technology*. John Wiley & Sons, Inc., Hoboken, New Jersey, third edition, 2009.
- [23] Asgari, S. Experimental study of the interaction between urea spray/wall. Master’s thesis, KTH Royal Institute of Technology, Chemical Engineering and Technology, November 2010.
- [24] Rapp, S. Quantitative analysis of FTIR measurements on urea and its decomposition products in an exhaust gas flow. Master’s thesis, KTH Royal Institute of Technology, Chemical Engineering and Technology, 2009.
- [25] Wedlund, J. Influence of spray characteristics on the evaporation and decomposition of a urea-water-solution. Master’s thesis, Chalmers University of Technology, 2012.